

Universality in quasinormal modes of a magnetized black hole

Marcos R. Ribeiro,^{1, a} Eveling C. Ribeiro,^{2, b} Kai Lin,^{3, c} and Elcio Abdalla^{2, 4, 5, d}

¹*Department of Mathematical Physics, Institute of Physics,
University of São Paulo, 05314-970 São Paulo, Brazil.*

²*Department of General Physics, Institute of Physics,
University of São Paulo, 05314-970 São Paulo, Brazil*

³*Federal University of Campina Grande, Campina Grande, PB 58429-900, Brasil*

⁴*Department of Physics, Center for Exact and Natural Sciences,
Federal University of Paraíba, 58059-970, João Pessoa, Brazil*

⁵*Paraíba State University, 351 Baraúnas Street, University District, Campina Grande, Brazil*
(Dated: December 10, 2025)

Black holes (BHs) in magnetized environments are a topic of intense research, both theoretical and observational. In particular, the interaction between charged matter and such objects provides a rich arena with applications ranging from fundamental field theory to high-energy astrophysics. In this work, we investigate the linear stability of a magnetized Einstein-Maxwell solution describing a static, axially symmetric BH immersed in a uniform magnetic field. We probe the dynamics of an external charged scalar field through its quasinormal modes (QNMs), combining frequency- and time-domain analyses. We find a critical value of the field charge at which the QNM spectrum exhibits universal power-law scaling with an exponent of approximately $1/2$. This critical behavior admits a simple interpretation in terms of a transition between a confined regime, where waves remain effectively trapped within a region of characteristic size $\sim 1/B$, and a deconfined regime, where the field reaches distances $\gg 1/B$ and the damping rate becomes parametrically small. These results provide qualitative and quantitative insights that may inform more realistic scenarios involving highly magnetized compact objects.

I. INTRODUCTION

A deep understanding of gravity remains a central goal of theoretical physics. In the classical regime, space-time dynamics is governed by general relativity via the Einstein field equations, which admit a wide variety of solutions of direct astrophysical relevance. For instance, the Schwarzschild solution and its generalizations describe spacetime around compact, spherically symmetric bodies with distinct properties [1–3], enabling theoretical studies of astrophysical objects such as stars and BHs.

Remarkably, BH have shifted from a purely theoretical subject to an important focus of observational astrophysics, especially with the detection of gravitational waves by the LIGO–Virgo Collaboration [4]. Such signals are expected not only from neutron-star collisions and BH mergers but also from primordial processes in the early Universe [5]. On the other hand, the Event Horizon Telescope team has provided images of the shadow of supermassive black holes at galactic centers [6]. Alongside these advances, radio observations have also proven to be a powerful means of probing the environment of compact objects, since cataclysmic events often produce detectable afterglows [7]. In this context, the BINGO radio telescope [8, 9] will provide a valuable opportunity to explore such radio signatures, contributing to a deeper understanding

of the astrophysical processes associated with compact objects.

BHs are often surrounded by accretion disks, which are made mostly of charged matter. The stability of this system is of high astrophysical interest, as it underlies many phenomena [10]. A particularly relevant case arises when a magnetic field permeates the compact object environment. These configurations have been discussed in connection with explosive events such as fast radio bursts [11, 12]. A complete theoretical solution of this problem is challenging and must self-consistently incorporate both gravity and relativistic plasma dynamics [13, 14]. Nevertheless, simplified models based on exact solutions of the Einstein–Maxwell equations provide a valuable starting point. This approach has been used by many authors and has yielded a number of interesting results [15–21].

F. J. Ernst developed in the 1970s a method for constructing exact non-asymptotically flat solutions of the Einstein–Maxwell equations from a previously known solution [22]. Over the years, these spacetimes have attracted considerable attention due to their potential astrophysical applications [16, 23–26]. The simplest example describes a static black hole immersed in a uniform magnetic field, namely the Ernst-Schwarzschild (ES) solution. In particular, [16] showed that this solution is stable under massless scalar perturbations. Moreover, these fields are confined to a region of order $\sim 1/B$ due to the presence of the magnetic field. Despite these important results, Ernst spacetimes remain relatively unexplored given their great potential for further applications.

In general relativity, critical behavior and universality can emerge in a striking way, signaling qualitative changes

^a marcosribeiro@usp.br

^b evelingmilena@usp.br

^c kailin@if.usp.br

^d eabdalla@usp.br

in a system's dynamics when a control parameter reaches a threshold value. A prominent example is the gravitational collapse studied by Choptuik and others [27, 28], where near-critical evolutions display universal scaling governed by a critical exponent. Related ideas also appear in black hole perturbation theory, where near-horizon geometry can exhibit an emergent conformal symmetry that organizes universal scaling patterns [29]. In the same context, it is well established that charged fields can cause instabilities under a variety of circumstances [17, 19]. This aspect is particularly relevant in astrophysical settings, where charged fields may naturally occur in the vicinity of realistic BHs. The propagation of charged scalar fields in the ES background was analyzed in [30]. Nevertheless, that study was restricted to the regime in which the parameter Br remains very small, thus neglecting the non-trivial asymptotic features inherent to the ES spacetime.

In this work, we investigate the propagation of charged scalar fields in the ES spacetime without relying on simplifying approximations. Our results show that, although magnetized BHs remain stable under charged scalar perturbations, the associated QNM spectrum exhibits a critical behavior at a threshold charge q_c . In the limit $q \rightarrow q_c$, the effective potential undergoes a qualitative topological change, leading to the deconfinement of the scalar field. We interpret this critical limit as a simplified mechanism that may serve as a toy model for emission processes.

The paper is organized as follows. In Section II, we briefly review the ES solution and its main features. In Section III, we study the dynamics of a charged scalar field in the ES spacetime and present the QNMs using two different approaches: direct integration (Sec. III B) and the time-domain profile (Sec. III C). Finally, in Section IV, we discuss our results and outline possible directions for future research.

II. BLACK HOLE IN A MAGNETIC FIELD

The ES spacetime is an axisymmetric solution of the Einstein–Maxwell equations, first discussed in [22]. It describes a static BH immersed in a uniform magnetic field. In geometric units ($G = c = 4\pi\epsilon_0 = 1$), the line element and the electromagnetic potential are given by

$$ds^2 = \Lambda^2 \left(f(r) dt^2 - \frac{dr^2}{f(r)} - r^2 d\theta^2 \right) - \frac{r^2 \sin^2 \theta}{\Lambda^2} d\phi^2, \quad (1)$$

$$A_\mu = -\frac{Br^2 \sin^2 \theta}{\Lambda} \delta_\mu^3, \quad (2)$$

where $f(r) = 1 - 2M/r$. The factor Λ depends on the parameter B as

$$\Lambda = 1 + B^2 r^2 \sin^2 \theta. \quad (3)$$

Here, B and M denote the strength of the external magnetic field and the total mass of the BH, respectively. Accordingly, the natural dimensionless parameter characterizing the ES solution is MB .

It is easy to note that in the limit of no external field $B \rightarrow 0$ we recover the Schwarzschild spacetime from the set of equations (1). In fact, the strength of the electromagnetic field plays a role of deforming the spherical symmetry, whose inverse defines a characteristic length. This means that the gravitational effect of the electromagnetic field is weaker when $r \ll 1/B$, however, it increases with distance from the BH. When $r \gg 1/B$ the deformation of the Schwarzschild geometry is extremely strong and the solution (1) approximates the Melvin universe [31, 32]. As a matter of fact, this feature ensures that the ES spacetime is not asymptotically flat when $B \neq 0$.

The external electromagnetic field does not change the position of the event horizon, which remains at $r = 2M$, but deforms its geometry due to the θ -dependence of Λ [33]. Indeed, in the axis of symmetry, the structure of the ES spacetime is similar to the Schwarzschild solution. On the other hand, out of the axis of symmetry we get a very peculiar geometry with many physical differences from the usual Schwarzschild BH [34, 35]. For instance, in the equatorial plane, the Gaussian curvature of the event horizon is negative when $BM > 1$ [33].

III. CHARGED SCALAR PERTURBATION

A. The perturbation equations

We consider the dynamics, in the ES background, of a charged scalar perturbation field Ψ which is minimally coupled to gravity via the standard action

$$S_\Psi = -\frac{1}{2} \int \sqrt{-g} d^4x \left(g^{\alpha\beta} \nabla_\alpha \Psi^* \nabla_\beta \Psi + \mu^2 \Psi^* \Psi \right), \quad (4)$$

where g is the determinant of the ES metric $g_{\alpha\beta}$, and ∇_α implements the minimal coupling between the charged field Ψ and the ES electromagnetic potential (2) via the replacement $\nabla_\alpha \rightarrow \nabla_\alpha + iqA_\alpha$.

The variational principle leads us to the equation of motion for scalar fields, which is simply the Klein-Gordon equation,

$$g^{\alpha\beta} (\nabla_\alpha + iqA_\alpha) (\nabla_\beta + iqA_\beta) \Psi + \mu^2 \Psi = 0. \quad (5)$$

Even though spherical symmetry is broken, a decomposition in terms of spherical harmonics is still useful. Thus, let us consider the following ansatz:

$$\Psi(t, r, \theta, \phi) = \frac{1}{r} \sum_{\ell, m} \psi_{\ell m}(r, t) Y_\ell^m(\theta, \phi). \quad (6)$$

where ℓ is the multipole number ($\ell = 0, 1, 2, \dots$) and m is the azimuthal number with $|m| \leq \ell$. Moreover, consider the orthogonality condition for the spherical harmonics:

$$\langle Y_\ell^m, Y_{\ell'}^{m'} \rangle = \int d\Omega Y_\ell^m(\theta, \phi) Y_{\ell'}^{m'*}(\theta, \phi) = \delta_{\ell\ell'} \delta_{mm'}, \quad (7)$$

where the integration is performed over the solid angle $d\Omega$.

Now, we can plug the ansatz (6) into Eq. (5) to obtain the following system of equations for each mode (ℓ, m) :

$$\frac{\partial^2 \psi_{\ell m}}{\partial r^2} + \frac{f'}{f} \frac{\partial \psi_{\ell m}}{\partial r} - \frac{1}{f^2} \frac{\partial^2 \psi_{\ell m}}{\partial t^2} - \frac{1}{f} \left(\frac{f'}{r} + \frac{\ell(\ell+1)}{r^2} \right) \psi_{\ell m} = \frac{1}{f} \sum_{\ell'} A_{\ell'}^{\ell'} \psi_{\ell' m} \quad (8)$$

The equation above is our master equation, which describes the dynamics of a charged scalar field in the ES spacetime. Note that our decomposition (6) results in a system of differential equations, where $A_{\ell'}^{\ell'}(r)$ couples different modes,

$$A_{\ell'}^{\ell'}(r) := f \langle Y_{\ell}^m, \Delta(r, \theta) Y_{\ell'}^m \rangle. \quad (9)$$

This is expected, as the magnetic field breaks the spherical symmetry. The explicit form of the function $\Delta(r, \theta)$ is given by:

$$\Delta = \frac{m^2 (\Lambda^4 - 1)}{r^2 \sin^2 \theta} + (q^2 B^2 r^2 \sin^2 \theta + \mu^2) \Lambda^2 - 2q m B \Lambda^3. \quad (10)$$

The matrix $A_{\ell'}^{\ell'}$ couples only modes with the same parity.

One can perform a change of variable to tortoise coordinates $r_* = \int dr/f(r)$ to obtain the wave-like equation from (8) as

$$\frac{\partial^2 \psi_{\ell m}}{\partial r_*^2} - \frac{\partial^2 \psi_{\ell m}}{\partial t^2} = V_{\text{eff}} \psi_{\ell m} + \sum_{\ell' \neq \ell} A_{\ell'}^{\ell'} \psi_{\ell' m} \quad (11)$$

where the effective potential is given by

$$V_{\text{eff}} = f \left(\frac{f'}{r} + \frac{\ell(\ell+1)}{r^2} \right) + A_{\ell}^{\ell}(r) \quad (12)$$

It is worth noting that the potential above is symmetric under the combined transformation $m \rightarrow -m$ and $q \rightarrow -q$. The effective potential has the standard barrier near the BH and is only weakly affected by the external magnetic field. However, the magnetic field becomes dominant in the asymptotic regime, as shown in Fig. 1. In fact, the asymptotic growth

$$\lim_{r \rightarrow \infty} V_{\text{eff}} \sim r^6, \quad (13)$$

ensures the confinement of any perturbation that satisfies (8). Nevertheless, due to the presence of electric charge in the scalar field, the asymptotic behavior can be smoothed out whenever $\mu = 0$ and $q = q_c := mB$. In this limit, the effective potential exhibits a quadratic growth similar to the AdS case with an "effective AdS radius" proportional to $1/B$, when mode coupling starts to be significant.

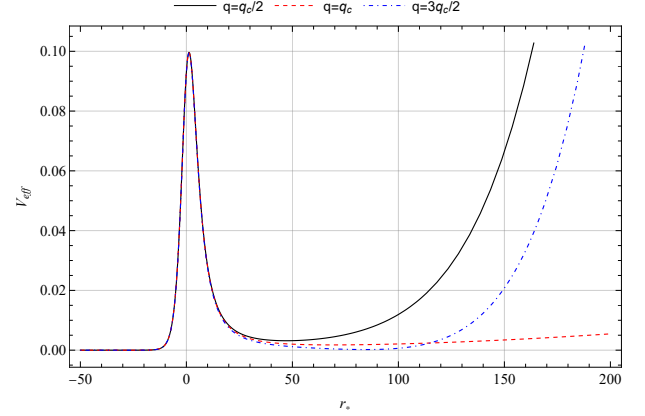


Figure 1: Effective potential for different values of the perturbation charge q . We set $BM = 0.02$, $\ell = m = 1$, and $\mu = 0$. Note that the growth at the critical charge q_c (red dashed) is weaker.

B. Frequency domain analysis

In this section, we compute the QNM associated with the perturbation equation (8). It is worth noting that the presence of an effective infinite wall (Fig. 1) leads to the appearance of long-lived modes in the quasi-normal spectrum. To find these modes, we assume a simplified, decoupled case, namely $A_{\ell'}^{\ell'} = 0$ for $\ell' \neq \ell$ in Eq. (8). Our analysis is carried out in the frequency domain, adopting a separable ansatz of the form $\psi_{\ell m} = R_{\ell m} e^{-i\omega t}$. In this analysis, we also assume the following asymptotic behavior

$$R_{\ell m}(r) \approx \begin{cases} e^{-i\omega r_*} & \text{as } r \rightarrow 2M \\ 0, & \text{as } r \gg 1/B \end{cases} \quad (14)$$

which represents an in-going wave at the event horizon and no waves far enough from BH.

The wave equation is given by

$$f \frac{d^2 R}{dr^2} + f' \frac{dR}{dr} - \left(\frac{f'}{r} - \frac{\omega^2}{f} + \frac{\ell(\ell+1)}{r^2} + A_{\ell}^{\ell} \right) R = 0. \quad (15)$$

Our strategy is to apply a direct numerical integration of Eq. (15) over the interval $I = [r_0, r_\infty]$, where the numerical parameters r_0 and $r_\infty \gg 1/B$ denote a region close to the black hole and a region far from it, respectively.

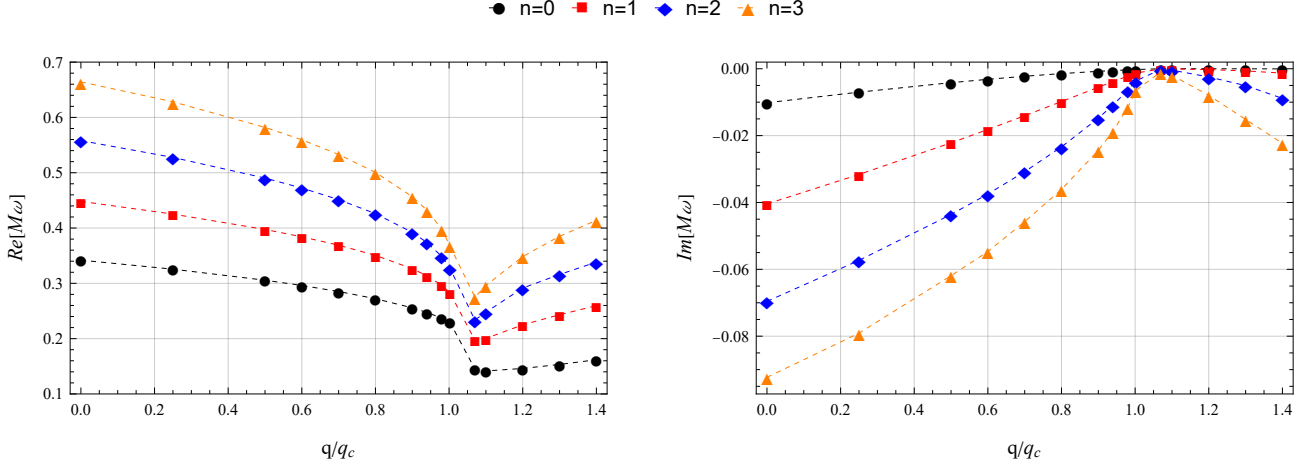


Figure 2: Quasi-normal spectrum of a massless perturbation as a function of the charge field normalized to the critical charge, q_c . The chosen parameters are $MB = 0.1$ with $\ell = m = 1$. We observe two distinct regimes, separated by the effective critical charge Q_c .

Close to the horizon, the solution behaves as

$$R \sim (r - 2M)^{-2iM\omega} \sum_n a_n (r - 2M)^n, \quad (16)$$

where $n > 0$, and the coefficients a_n are determined in terms of $a_0 = 1$ by solving Eq. (15) order by order. The QNMs are obtained by imposing the second boundary condition given in Eq. (14), which leads to an equation satisfied only by a discrete set of complex frequencies.

We performed a detailed numerical analysis of the QNM spectrum, which can be defined as a set of the kind $\omega_{n\ell m}$, as a function of B , and q , with representative results shown in Fig. 2. Our numerical scheme exhibits reduced stability in the interval $q/q_c \in I_c \approx [1, 1.1]$, with this window narrowing on the right as the overtone index n increases. For this reason, there is a small gap in Fig. 2. In addition, we identify a special charge value Q_c , with $Q_c/q_c \in I_c$, at which the QNM behavior abruptly reverses. The real part of the quasinormal frequency (left panel of Fig. 2) decreases with the field charge for $q < Q_c$ across all parameter values considered, whereas in the second regime, $q > Q_c$, it increases. Notably, both regimes obey a power-law scaling for the real frequency of the form

$$\text{Re}[\omega] = \omega_c^\pm + \beta^\pm |q - Q_c|^{\gamma^\pm}, \quad (17)$$

where ω_c , β , γ , and Q_c are positive numerical coefficients. We denote the critical frequency by $\omega_c^\pm := \text{Re}\omega(Q_c)$. To avoid making premature assumptions, we allow the coefficients to differ on the two sides, writing the superscript \pm which labels the first ($q < Q_c$) and second ($q > Q_c$) regimes, respectively.

We observe that Q_c is not a single value, rather, it depends on the mode. We find a strong dependence on both the azimuthal number and the magnetic-field parameter.

n	γ^-	γ^+	Q_c
0	0.50		0.1046
1	0.42		0.1028
2	0.42	0.52	0.1020
3	0.44	0.45	0.1016

Table I: Numerical values for the effective critical charge and exponents for $MB = 0.1$. In this analysis, we obtained errors of at most 7% and 0.5% for γ^\pm and Q_c respectively. Our numerical analysis is less stable on the right side, especially for small n , which explains the absence of these values.

This behavior is expected since Q_c represents a small deviation from the critical charge $q_c = mB$. For instance, Q_c is approximately 2.4 times larger when comparing the modes ω_{021} and ω_{022} , with B fixed. On the other hand, we find little dependence on ℓ or n . Remarkably, Q_c approaches q_c as the overtone number n increases, as shown in Table I.

The numerical calculations for the exponents γ^\pm are also reported in Table I for the case $MB = 0.1$. However, for all modes tested at different values of $MB \ll 1$, the exponent remains within the error bars across these cases. This numerical evidence motivates us to regard it as universal, and we obtain a remarkably good fit in both regimes ($q \gtrless Q_c$), with $\gamma^\pm \approx 0.46$. We observe that, at the critical point, the spectrum seems to bifurcate and new modes emerge. As a result, there is a natural gap in our system, which in turn requires distinct values for the numerical parameters for the different regimes. Specially, the critical frequency in the first regime is consistent with the following behavior

$$\omega_c^- \sim (0.35n + 0.036\ell + 1.6m + 0.39) B. \quad (18)$$

On the second-regime side, our numerical calculation is

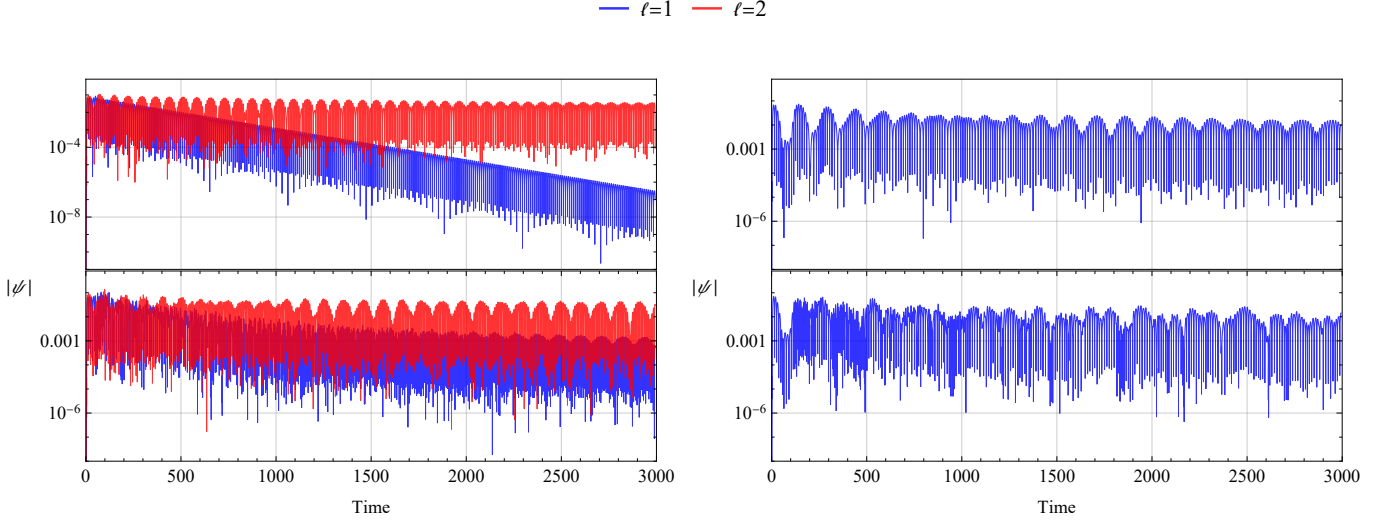


Figure 3: Time-domain profiles (top: decoupled; bottom: coupled with $\ell_{\max} = 5$) for $m = 1$, and $BM = 0.1$. Left: $\ell = 1, 2$, $q/q_c = 0.5$; right: $\ell = 1$, $q/q_c = 1.08$. The decay rate decreases not only with increasing multipole number, but also as the critical charge is approached.

n	ξ^-	ξ^+	Q_c
0	0.96		0.1046
1	0.90		0.1028
2	0.74	1.89	0.1020
3	0.62	1.78	0.1016

Table II: Numerical values for the effective critical charge and exponents for $MB = 0.1$ with $\ell = m = 1$. In this analysis, we obtained errors of at most 4%. The reason for omitting the initial n values is the same as in the previous table.

less stable and the uncertainties are larger, so the data do not provide enough sensitivity to reliably determine the parameter dependence of ω^+ in this regime. Despite this, within the parameter space explored, the critical frequency shows no significant variation and remains approximately constant. For $MB = 0.1$ we found it around $\omega_c^+ \approx 0.19$. The parameter β is always of order unity, increasing with B and n and decreasing with m .

The behavior of the imaginary part, shown on the right in Fig. 2, exhibits a similar change in behavior in the transition from the first to the second regime. In particular, very close to Q_c , all modes become approximately equal and display a very small decay rate, indicating a quasi-degenerate state of the system. The imaginary part also follows a power-law behavior of the form

$$\text{Im}[\omega] = -\zeta^\pm |q - Q_c|^{\xi^\pm}, \quad (19)$$

where ζ and ξ are positive numerical parameters. Here Q_c denotes the same critical charge as in the real part. Unlike $\text{Re}[\omega]$, the exponent governing the imaginary contribution depends nontrivially on n , ℓ , and m . For the special case

$\ell = m = 1$, Fig. 2 shows a clear change in the concavity of the mode curve for different overtone numbers in the first regime. Indeed, we observe a small decrease in the exponent ξ^- , with a possible plateau at large n , similar to what we found for Q_c . That is, we expect the exponent to satisfy a relation of the form

$$\xi^\pm = \xi_0^\pm + f(n, \ell, m), \quad (20)$$

such that $\lim_{n \gg 1} f = 0$. However, due to the lack of numerical results in $n \gg 1$, we cannot reliably determine either the asymptotic value or the functional form of f . Assuming a rational dependence, we obtain for the first regime, from the data in Fig. 2,

$$\xi^- \approx 0.34 + \frac{1.1}{1+n}. \quad (21)$$

C. Time domain analysis

In this section, we present the results obtained from a time-domain analysis of the system described by (11). We consider the general case where different modes are coupled in the region $r \sim 1/B$. Thus, in our numerical integration, we introduce a multipole cutoff ℓ_{\max} in such a way that $A_{\ell'}^{\ell} = 0$ for $\ell' > \ell_{\max}$. As an initial condition, we consider a Gaussian wave packet, $\psi(0, r) = \sqrt{2/\pi} \exp[-\kappa(r - r_0)^2]$, falling into the BH. Spatial derivatives are approximated using a fourth-order accurate central finite difference scheme, while time evolution is computed via a second-order explicit method. The corresponding finite difference expressions for the second-order derivatives in time and space are given by,

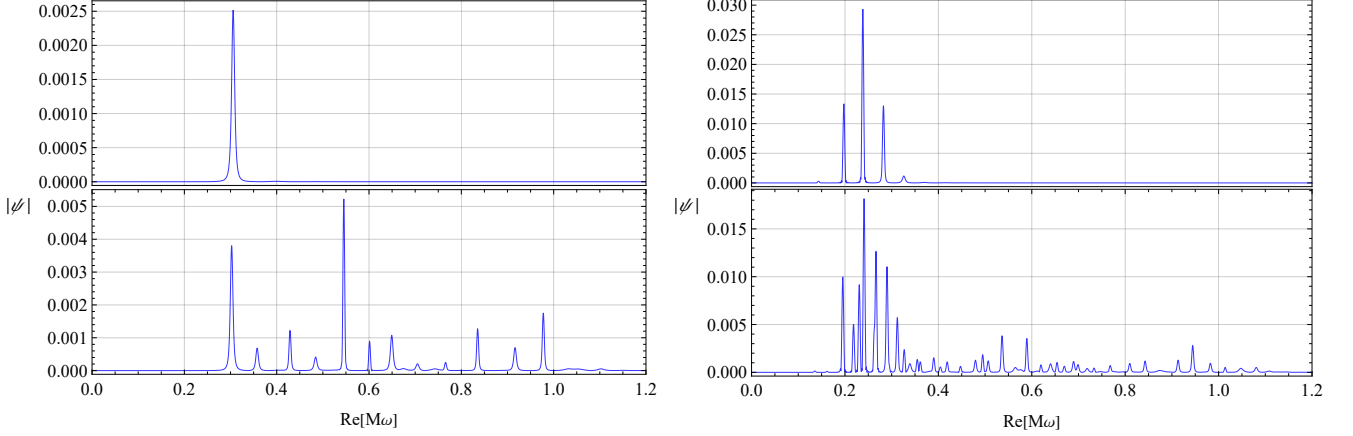


Figure 4: Fourier spectrum for the simulations shown in Fig. 3 for $\ell = 1$. Far from the critical charge, we observe only the fundamental mode (top left). However, as we approach q_c , additional modes are excited, producing an echo-like profile (top right). When we take the coupling into account (bottom panels), we observe echoes even far from the critical charge (left), as well as an increase in the number of excited frequencies near the critical charge (right). Moreover, close to the critical charge we find that the lowest-lying modes have an extremely small imaginary part in the decoupled case, and an even smaller one in the coupled case.

$$\partial_{r_*}^2 \psi_{i,j} = \frac{1}{12\Delta r_*^2} \left(-\psi_{i-2,j} + 16\psi_{i-1,j} - 30\psi_{i,j} + 16\psi_{i+1,j} - \psi_{i+2,j} \right) \quad (22)$$

and

$$\partial_t^2 \psi_{i,j} = \frac{1}{\Delta t^2} \left(\psi_{i,j+1} - 2\psi_{i,j} + \psi_{i,j-1} \right). \quad (23)$$

As noted in Section III, the perturbation remains confined to a finite spatial region due to the asymptotic behavior of the effective potential for large Br . This means that very close to the black hole, the perturbation oscillations resemble those of the massive Schwarzschild QNMs, where the effective mass is given by $\mu_{\text{eff}}^2 = \mu^2 + 2|qmB|$. Nevertheless, after a time of order $t \sim 1/B$, the wave interacts with the effective wall barrier, producing long-lived modes and exhibiting an echo-like structure, as shown in Fig. 3.

For the sake of illustration, in Fig. 4 we show the real frequencies for $MB = 0.1$ at two different charges: one far from and one close to q_c , using multipole cutoffs $\ell_{\text{max}} = 1$ and 5. Note that the initial Gaussian packet gradually excites additional modes. This is expected because, in the limit $q \rightarrow q_c$, the effective potential changes, leading to a further outward displacement of the effective barrier into the region $r \gg 1/B$. This provides intuition for the very small decay rates found in the previous section for small n . Moreover, we observe that the coupled case yields decay rates that are much smaller than those of the decoupled cases, which strongly suggests a transition

from a decaying to a non-decaying mode, marked by

$$\lim_{q \rightarrow q_c} \text{Im}[\omega] \approx 0. \quad (24)$$

Across the transition at $q \approx q_c$, we observe a discontinuity in the spectrum accompanied by the emergence of new modes. For instance, in Fig. 4 (right) a new fundamental mode appears at $\text{Re}[\omega_{011}] \approx 0.14$. Furthermore, in the coupled case we observe a narrower typical spacing between consecutive frequencies, $|\omega_{n+1} - \omega_n| \sim 0.2B$.

IV. DISCUSSION

A. Scaling law

The wave propagating around the Ernst BH is effectively confined by the asymptotic behavior of the space-time at infinity. This setup leads to a dynamics analogous to that of a small perfect absorber placed inside a confining box. It was shown in Ref. [16] that, in such systems, the real part of the QNM frequency scales inversely with the effective box radius r_0 . In our analysis, we find that the presence of charge introduces a second characteristic length scale, which displays a critical dependence on the scalar field charge, given by

$$d \sim |q - q_c|^{-\gamma}. \quad (25)$$

To see this, we consider the characteristic length scale d at which the quadratic growth

$$V_{\text{eff}}(r, q_c) \sim B^4 r^2 \quad (26)$$

starts to compete with the quartic contribution induced by a small deviation of the charge, $q = q_c + \epsilon$, with $|\epsilon| \ll 1$. In other words, we evaluate

$$\delta V_{\text{eff}}(d; \epsilon) := |V_{\text{eff}}(d; q_c + \epsilon) - V_{\text{eff}}(d; q_c)| \sim B^4 d^2. \quad (27)$$

The relation above leads to the following scaling law for the characteristic length (d):

$$d \sim |\epsilon|^{-1/2} (a_0 + a_1 \epsilon + O(\epsilon^2)), \quad (28)$$

where a_0 and a_1 are coefficients that depend on the background parameter B . This length diverges as $\epsilon \rightarrow 0$, indicating critical behavior with a scaling exponent of $1/2$. Therefore the scaling law for the real frequency is

$$\text{Re}[\omega] \sim |q - q_c|^{1/2}. \quad (29)$$

Notice that this analysis is mode-independent. Thus, it suggests universality and is consistent with the scaling we found numerically in Sec. III B. The $\sim 8\%$ error is due to the lack of numerical data in the critical region I_c .

B. Final Remarks

Throughout this work, we have argued that charged bosonic fields near magnetized BH can undergo a phase transition when they reach a critical charge. Conceptually, this transition is characterized by a change from a confined state, in which the waves remain close to the BH, to a deconfined phase in which the wave escapes to regions far from the BH. Quantitatively, we find strong numerical evidence for critical behavior, marked by a universal critical exponent of approximately $1/2$ for the real frequency. On the other hand, although we do not yet have sufficient numerical evidence for universal behavior in the imaginary part, it becomes virtually zero, suggesting a genuinely special state of the system. In this way, the results presented in this work provide an interesting example of nontrivial behavior obtained from a purely linear analysis of interaction between magnetized BH and charged field. This also suggests that immediate extensions, such as including BH rotation or backreaction effects may broaden these results and lead to possible real applications, given the frequent occurrence of systems involving black holes and magnetic fields in our Universe.

Any application of the ES solution to astrophysical situations must be treated with caution due to its non-asymptotically flat behavior at infinity. Nevertheless,

accretion discs can sustain large scale magnetic fields [36], thereby magnetizing a black hole. In this spirit, the ES solution may be used at least as an approximation up to some finite distance L , especially in scenarios where such magnetic fields provide a confinement/trapping mechanism [37]. With these caveats in mind, we can convert our results to physical units, as discussed in this work.

We perform a detailed analysis in the regime $MB \leq 10^{-1}$. Restoring SI units, the corresponding magnetic field scale is

$$B_{\text{phys}} \sim 10^{14} \left(\frac{M_{\odot}}{M} \right) \text{ T}, \quad (30)$$

where M_{\odot} is the solar mass. This is far above the largest fields inferred for magnetars, typically $B_{\text{mag}} \sim 10^{-4} B_{\text{phys}}$.

One of the most important result of this work is that the critical frequency has a non null value given by Eq. (18). We interpret this fact as the characteristic frequency of a signal that can propagate to large distances. Therefore, the phase transition can be thought of as an emission threshold limit in which the bosonic waves are transmitted. The frequency of this signal for magnetic fields of order B_{mag} , has the following magnitude

$$\nu_c \sim 3.2 \times 10^{-1} \left(\frac{M_{\odot}}{M} \right) \text{ Hz}. \quad (31)$$

This is negligibly small for stellar mass BH, but it can be larger for small mass. In particular, light primordial black holes are considered as a fraction of dark matter and their interaction with a neutron star is considered as a possible FRB engine [38]. For instance, taking $M \sim 10^{25} \text{ g}$ [39] yields¹ $\nu_c \sim 1.6 \text{ GHz}$. In that case, we come near the size of a progenitor of a Fast Radio Burst [11]. We conclude that such simple models might cope with more sophisticated phenomena [40, 41].

ACKNOWLEDGMENTS

The authors acknowledge the funding support provided by the following agencies: Fapesp, grant 2014/07885-0 (EA); CNPq, grants 303592/2020-6 (EA), 141276/2021-5 (MRR), 141310/2024-3 (ECR). The authors also thank Alberto Saa for reading the manuscript and for useful discussions.

¹ However, it is not clear what the mass of a primordial Black Hole is. For lighter primordial BH the critical frequency can raise this figure to ultraviolet range.

[1] K. Schwarzschild, On the gravitational field of a mass point according to einstein's theory (1999), [arXiv:physics/9905030](https://arxiv.org/abs/physics/9905030).

- [2] H. Stephani, D. Kramer, M. MacCallum, C. Hoenselaers, and E. Herlt, *Exact solutions of Einstein's field equations* (Cambridge university press, 2009).
- [3] J. B. Griffiths and J. Podolskỳ, *Exact space-times in Einstein's general relativity* (Cambridge University Press, 2009).
- [4] B. Abbott, R. Abbott, T. Abbott, *et al.*, Phys. Rev. Lett. **116**, 061102 (2016), [arXiv:1602.03837](#).
- [5] M. C. Guzzetti, N. Bartolo, M. Liguori, *et al.*, Riv. Nuovo Cim. **39**, 399 (2016), [arXiv:1605.01615](#).
- [6] E. H. T. Collaboration, K. Akiyama, A. Alberdi, *et al.*, Astrophys. J. Lett. **930**, L14 (2022), [arXiv:2311.09479](#).
- [7] G. Hallinan, A. Corsi, K. Mooley, *et al.*, Science **358**, 1579 (2017), [arXiv:1710.05435](#).
- [8] E. Abdalla, E. G. Ferreira, R. G. Landim, *et al.*, A&A **664**, A14 (2022), [arXiv:2107.01633](#).
- [9] M. V. dos Santos, R. G. Landim, G. A. Hoerning, *et al.*, A&A **681**, A120 (2024), [arXiv:2308.06805](#).
- [10] R. D. Blandford and D. Payne, Mon. Not. Roy. Astron. Soc. **199**, 883 (1982).
- [11] B. Zhang, Nature **587**, 45 (2020), [arXiv:2011.03500](#).
- [12] C. D. Bochenek, V. Ravi, K. V. Belov, *et al.*, Nature **587**, 59 (2020), [arXiv:2005.10828](#).
- [13] O. Korobkin, E. B. Abdikamalov, E. Schnetter, *et al.*, Phys. Rev. D **83**, 043007 (2011), [arXiv:1011.3010](#).
- [14] S. A. Balbus and J. F. Hawley, Rev. Mod. Phys. **70**, 1 (1998).
- [15] R. Konoplya and A. Zhidenko, Phys. Rev. D **73**, 124040 (2006), [arXiv:gr-qc/0605013](#).
- [16] R. Brito, V. Cardoso, and P. Pani, Phys. Rev. D **89** (2014), [arXiv:1405.2098](#).
- [17] A. A. A. Filho, K. Jusufi, B. Cuadros-Melgar, *et al.*, Phys. Dark Univ. **46**, 101711 (2024), [arXiv:2401.15211](#).
- [18] K. Lin, Y. Liu, W. L. Qian, *et al.*, Phys. Rev. D **100**, 065018 (2019), [arXiv:1909.04347](#).
- [19] Z. Zhu, S. J. Zhang, C. Pellicer, *et al.*, Phys. Rev. D **90** (2014), [arXiv:1405.4931](#).
- [20] E. C. Ribeiro, L. Formigari, M. R. Ribeiro, Jr., *et al.*, Phys. Rev. D **111**, 024043 (2025), [2411.11117](#).
- [21] V. P. de Freitas and A. Saa, Phys. Rev. D **95** (2017), [arXiv:1703.10883](#).
- [22] F. J. Ernst, J. Math. Phys. **17**, 54 (1976).
- [23] S. Shaymatov, M. Jamil, K. Jusufi, *et al.*, Eur. Phys. J. C **82**, 636 (2022), [arXiv:2205.00270](#).
- [24] K. R. Nayak and C. Vishveshwara, Gen. Relativ. Gravit. **29**, 291 (1997).
- [25] R. Konoplya and R. Fontana, Phys. Lett B **659**, 375 (2008), [arXiv:0707.1156](#).
- [26] G. T. Horowitz and H. J. Sheinblatt, Phys. Rev. D **55**, 650 (1997), [arXiv:gr-qc/9607027](#).
- [27] M. W. Choptuik, Phys. Rev. Lett. **70**, 9 (1993).
- [28] L. R. Werneck, Z. B. Etienne, E. Abdalla, *et al.*, Class. Quantum Grav. **38**, 245005 (2021), [arXiv:2106.06553](#).
- [29] S. E. Gralla and P. Zimmerman, JHEP **2018** (6), 1, [arXiv:1804.04753](#).
- [30] R. Bécár, P. González, and Y. Vásquez, Eur. Phys. J. C **83**, 75 (2023), [arXiv:2211.02931](#).
- [31] M. A. Melvin, Phys. Lett. **8**, 65 (1964).
- [32] K. S. Thorne, Phys. Rev. **139**, B244 (1965).
- [33] W. J. Wild and R. M. Kerns, Phys. Rev. D **21**, 332 (1980).
- [34] N. Dadhich, C. Hoenselaers, and C. Vishveshwara, J. Phys. A Gen. Phys. **12**, 215 (1979).
- [35] Z. Stuchlík and S. Hledík, Class. Quant. Grav. **16**, 1377 (1999), [arXiv:0803.2536](#).
- [36] R. Narayan, I. V. Igumenshchev, and M. A. Abramowicz, Astron. Soc. Jap. **55**, L69 (2003), [arXiv:astro-ph/0305029](#).
- [37] M. Romanova, G. Ustyugova, A. Koldoba, *et al.*, Astrophys. J. **500**, 703 (1998).
- [38] M. A. Abramowicz, M. Bejger, and M. Wielgus, Astrophys. J. **868**, 17 (2018), [arXiv:1704.05931](#).
- [39] J. Auffinger, Prog. Part. Nucl. Phys **131**, 104040 (2023), [arXiv:2206.02672](#).
- [40] X. Zhang, Y. Sang, G. A. Hoerning, *et al.*, Astrophys. J. **991**, 189 (2025), [arXiv:2411.17516](#).
- [41] M. V. dos Santos, R. G. Landim, G. A. Hoerning, *et al.*, A & A **681**, A120 (2024), [arXiv:2308.06805](#).